View Article Online / Journal Homepage / Table of Contents for this issue

JOURNAL OF Materials CHEMISTRY

Growth and form of gold nanorods prepared by seed-mediated, surfactant-directed synthesis

Christopher J. Johnson,[a] Erik Dujardin,[a] Sean A. Davis,[a] Catherine J. Murphy[b] and Stephen Mann*[a]

[a]*School of Chemistry, University of Bristol, Bristol, UK BS8 1TS. E-mail: s.mann@bris.ac.uk*
[b]*Department of Chemistry and Biochemistry, University of South Carolina, 631 Sumter Street, Columbia, SC 29208, USA*

Received 24th January 2002, Accepted 21st March 2002
First published as an Advance Article on the web 16th April 2002

Published on 16 April 2002. Downloaded by Pennsylvania State University on 12/09/2016 10:55:22.

Gold nanorods were prepared *via* a seed-mediated sequential growth process involving the use of citrate-stabilised seed crystals and their subsequent growth in a series of reaction solutions containing $[AuCl_4]^-$, ascorbic acid and the cationic surfactant cetyltrimethylammonuim bromide (CTAB). Electron diffraction analysis and HRTEM images of mature nanorods showed superpositions of two specific pairs of crystallographic zones, either <112> and <100> or <110> and <111>, which were consistent with a cyclic penta-twinned crystal with five {111} twin boundaries arranged radially to the [110] direction of elongation. The nanorods have an idealised 3-D prismatic morphology with ten {111} end faces and five {100} or {110} side faces, or both. TEM studies of crystals at various stages of growth indicated that the seed crystals are initially transformed by growth and aggregation into decahedral penta-twinned crystals, 4% of which become elongated when a fresh reaction solution is added, whilst the remaining twins grow isometrically. Reiteration of this procedure increases the length of the existing nanorods, induces further transformation of isometric particles to produce a second (and third) population of shorter, wider nanorods, and increases the size of the isometric crystals. The data indicate that symmetry breaking in fcc metallic structures to produce anisotropic nanoparticles is based on an intrinsic structural mechanism (twinning) that is subsequently modulated extrinsically during growth in solution by specific adsorption of Au^{I}–surfactant complexes on the side faces/edges of the isometric penta-twinned crystals and which is responsible for the preferential growth along the common [110] axis. We propose that the coupling of multiple twinning and habit modification is a general mechanism that applies to other experimental procedures (electrochemical, inverse micellar media) currently used to prepare metallic nanoparticles with a high aspect ratio.

Introduction

The self-assembly of inorganic nanoparticles into superlattices and nanostructures offers the potential to fabricate materials with tunable physical and chemical properties.[1,2] Ultimately, the collective behaviour of these superstructures is dependent on the design and control of the shape, size and spatial organization of the building blocks, and the chemistry and structure of interparticle spacer molecules. At present, many of these architectures, such as hexagonal close packed 2-D[3,4] and 3-D superlattices,[5] and ringed structures,[6,7] reflect the isotropic nature of their constituent nanoparticles. A surprising exception is the formation of wire-like assemblies of spherical silver nanocrystals formed spontaneously at the air/water interface.[8] In general, the fabrication of anisotropic nanostructures can be achieved using isotropic nanoparticles provided that these are confined within anisotropic environments, such as printed micro-architectures,[9] helicoid biolipid tubules[10] and block copolymers.[11] Alternatively, the reduced symmetry of nanoparticles with shape anisotropy can be transferred directly to analogous superlattice architectures even in the presence of isotropic interactions.[12–14]

In principle, the synthesis of anisotropic nanoparticles is relatively straightforward for non-cubic crystal structures, for example, hexagonal CdSe,[15,16] whereas symmetry breaking is required for structurally isotropic materials such as face-centred cubic (fcc) metals. Thus it is somewhat surprising that there have been several recent reports describing the synthesis of rod-shaped nanoparticles of gold,[17–21] silver,[22,23] copper[24] and nickel[25] with fcc structures. Moreover, these materials have been prepared by diverse methods including seed-mediated,[17,22] electrochemical[19] and biological[21] reduction in aqueous solutions, gas phase deposition,[23] and reduction of copper salts in water-in-oil microemulsions.[24] In each case, the shape anisotropy was considered to arise from template-directed processes that physically constrain crystal growth; for example, along the stepped surfaces of a NaCl crystal[23] or within or on the surface of elongated surfactant micelles.[18,24] In addition, several reports indicate that the rod-shaped nanoparticles can be twinned – for example, a low percentage of the gold nanorods prepared by electrochemical procedures or bioreduction were shown to be twinned along a single {111} twin plane,[21,26] whereas copper nanorods prepared in microemulsions and silver nanorods grown on NaCl stepped surfaces exhibited five-fold twinning[22,27] – although no mechanistic details were reported.

In this paper we use electron diffraction analysis and electron microscopy to determine the structure of gold nanorods prepared by seed-mediated surfactant-directed synthesis, and the stages of growth responsible for the onset and development of the shape anisotropy. The experimental method involves the use of citrate-stabilised Au nanoparticles and their subsequent growth in a series of aqueous solutions containing $[AuCl_4]^-$, ascorbic acid and the cationic surfactant cetyltrimethylammonuim bromide (CTAB).[17] Because primary nucleation is curtailed under these conditions, the transformation of the seeds to Au nanorods can be readily determined by structural and morphological analysis of samples obtained from the reaction sequence at different times.

This journal is © The Royal Society of Chemistry 2002

View Article Online

Published on 16 April 2002. Downloaded by Pennsylvania State University on 12/09/2016 10:55:22.

Experimental

Gold nanorods were prepared *via* a surfactant-containing, seed-mediated sequential growth process as previously described.[17] Briefly, 10 ml of citrate-stabilised gold nanoparticles (seed crystals) were prepared by reduction of a 10 ml solution containing 0.25 mM $[HAuCl_4]\cdot 3H_2O$ and 2.5 mM citric acid with 0.3 ml of ice cold aqueous 0.1 M $NaBH_4$. 9 ml of an aqueous growth solution containing 0.1 M CTAB and 0.25 mM $[HAuCl_4]\cdot 3H_2O$ were poured into each of four test-tubes. Addition of the CTAB produced a colour change from yellow to brown-yellow suggesting the presence of ligand-substituted anions such as $[AuCl_3Br]^-$, or CTAB–Au(III) complexes, or both. 50 µl of 0.1 M ascorbic acid, followed by 1 ml of the original solution containing the seed crystals, were added to one of the tubes (tube 1). Addition of the ascorbic acid turned the solution from brown-yellow to colourless suggesting that the Au(III) complexes were initially reduced to aqueous Au(I) anions,[28] such as $[AuCl_2]^-$, rather than Au (0). The mixture was left for 24 h before similarly reducing the Au (III) solution in a second test-tube (tube 2) with ascorbic acid, and then adding 1 ml of the aged solution from tube 1. This procedure was then repeated after a further 24 h such that successive transfers of 1 ml of aged solutions into freshly reduced solutions proceeded from tube 2 to 3, and then from 3 to 4. Doubly distilled water was used throughout the experiments and all glassware was cleaned with *aqua regia*.

Excess CTAB was removed from the nanoparticles by centrifuging 1 ml of the dispersions at 24 °C and 13 200 rpm, 16 100 rcf, for up to 60 min. The particles were collected, re-dispersed in 1 ml of water by sonication and re-centrifuged, and finally suspended in 0.2 ml of water. Samples were prepared for high resolution transmission electron microscopy (HRTEM) studies by depositing one drop (50–100 µl) of the dispersion onto carbon-coated copper mesh grids and air-drying for a day. Low magnification TEM images were recorded on a JEOL 1200 analytical electron microscope operating at 120 kV accelerating voltage. A JEOL 2010 electron microscope operating at 200 kV was used to record selective area electron diffraction (SAED) patterns and high resolution lattice images. Particle size distributions and corresponding statistical analyses of different morphological types of gold nanoparticles observed in tubes 1 to 4 were obtained from TEM images, either by measuring directly from photographic prints or by using analySIS software to measure digital images. In each case, at least 200 particles were counted, and approximately 800 particles were measured for the rod-shaped crystals formed in tubes 3 and 4.

Results

Structure and morphology

The crystallographic structure and 3-D crystal morphology of individual gold nanorods prepared by seed-mediated sequential growth in the presence of CTAB were determined by SAED in combination with HRTEM. At zero degree tilt, not all the rods imaged on the TEM grid showed Bragg diffraction. Of those that did, SAED gave two types of patterns in equal proportions (Fig. 1 and 2). Neither pattern could be indexed as a single

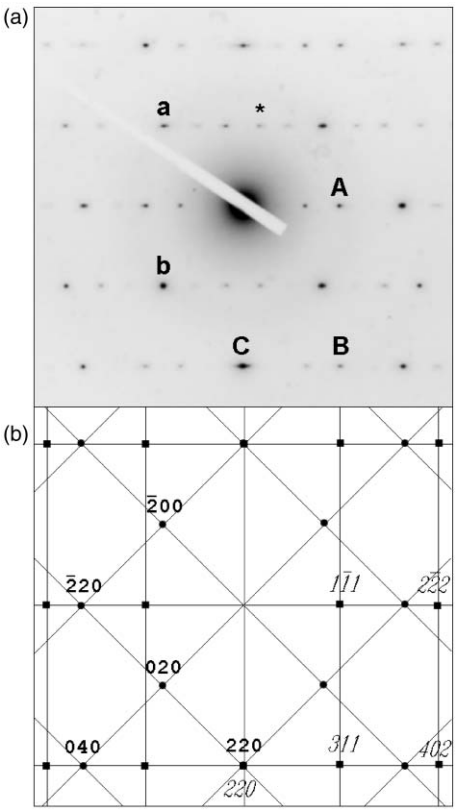

Fig. 1 (a) Electron diffraction pattern of gold nanorods corresponding to a superposition of rectangular <112> and square <100> zone patterns of a face-centred cubic structure (*Fm*3*m*, a = 0.4078 nm) and associated double diffraction reflections. See text for details. (b) Schematic showing superimposed [$\bar{1}$12] and [001] reciprocal lattices and indexed reflections in italics and bold typeface, respectively. Interplanar spacings: d_{111} = 0.2355, d_{220} = 0.1442, d_{222} = 0.1177, d_{200} = 0.2039, d_{220} = 0.1442, d_{113} = 0.1230, d_{400} = 0.1020, and d_{420} = 0.0912 nm. Interplanar angles: $(1\bar{1}1) \wedge (311) = 58.5°$, $(1\bar{1}1) \wedge (220) = 90°$, $(\bar{2}00) \wedge (020) = 90°$, $(020) \wedge (220) = 45°$.

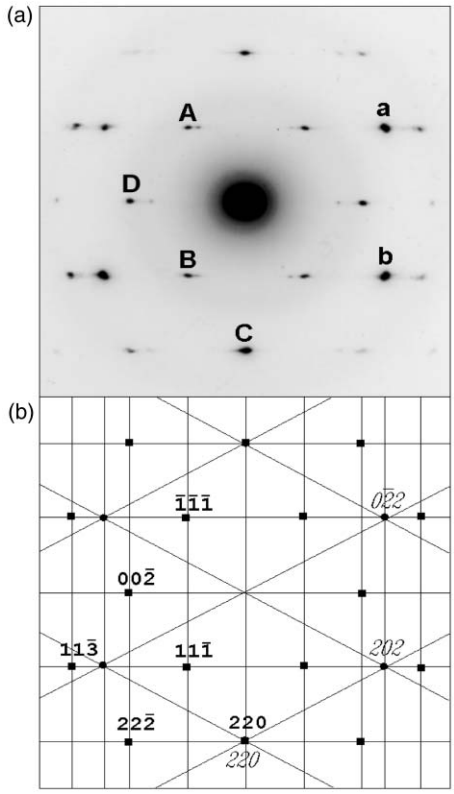

Fig. 2 (a) Electron diffraction pattern of gold nanorods corresponding to the superposition of <110> and <111> zones of a face-centred cubic structure. The first order reflections in the rectangular [$1\bar{1}0$] pattern (labelled A, B, C and D) correspond respectively to the $(\bar{1}\bar{1}\bar{1})$, $(11\bar{1})$, (220) and $(00\bar{2})$ planes, shown schematically in bold typeface in (b). The pattern is overlaid with a larger hexagonal reciprocal lattice (labelled a, b and C) indexed respectively in italics as the $(0\bar{2}2)$, (202) and (220) reflections of the [$1\bar{1}1$] zone. Reflections from multiple diffraction are also present. Interplanar spacings are given in the legend of Fig. 1. Interplanar angles: $(\bar{1}\bar{1}\bar{1}) \wedge (11\bar{1}) = 109.5°$, $(11\bar{1}) \wedge (220) = 35.3°$, $(\bar{1}\bar{1}\bar{1}) \wedge (00\bar{2}) = 54.7°$, $(0\bar{2}2) \wedge (202) = 60°$.

View Article Online

Published on 16 April 2002. Downloaded by Pennsylvania State University on 12/09/2016 10:55:22.

zone, indicating that the gold nanorods were not single domain crystals. Instead, both types of pattern consisted of a superposition of two specific crystallographic zones of general form, <112> and <100> (Fig. 1), and <110> and <111> (Fig. 2), which were consistent with multiple twinning of a face-centred cubic structure. For example, the first order reflections in the [$\bar{1}$12] zone shown in Fig. 1(a) correspond to the (1$\bar{1}$1), (311) and (220) planes (labelled A, B, C, respectively) and generate a rectangular reciprocal lattice [Fig. 1(b)]. This is overlaid with a square lattice corresponding to the [001] zone with ($\bar{2}$00), (020) and (220) reflections [labelled as a, b and C, respectively, in Fig 1(a)]. The mutual orientation of these two zones accounts for the numerous additional reflections seen in Fig. 1(a), which arise from double diffraction. For example, the spot marked with an asterisk in Fig. 1(a) corresponds to the vector sum (***a*** + ***A***). A similar analysis of the second type of observed electron diffraction pattern, which corresponded to the superposition of <110> and <111> zones, is shown in Fig. 2.

Both types of composite electron diffraction patterns can be rationalised on the basis that the gold nanorods consist of an elongated variant of a cyclic penta-tetrahedral twin crystal in which five {111} twin boundaries are arranged radially to the direction of elongation. This type of twinning is common in isotropic gold nanoparticles with decahedral (D_{5h}) morphology[29] because the interfacial angle between {111} planes (70.53°) is close to 2π/5 (72°). In the case of the nanorods, the shape anisotropy originates from a specific elongation along the common [110] five-fold axis to produce an idealised 3-D morphology based on a pentagonally twinned prism with five {100} side faces and capped at both ends by five {111} faces (Fig 3a). The absence of any preferred zone combination in the electron diffraction patterns, however, suggests that the side faces of the nanorods are either not well-developed and are therefore rounded, or consist of two forms, *viz.* {100}and {110}, of approximately equivalent surface area.

Each twin domain consists of a uniaxially elongated distorted tetrahedron of {111} faces such that the nanorods have a pentagonal cross-section when viewed along the common [110] axis with five face-sharing, symmetry-related tetrahedral sub-units, labelled as T1 to T5 in Fig. 3b. This arrangement limits the number of observable Bragg diffraction orientations arising from crystals mounted on the TEM grids to two possibilities [Fig. 3b, (i) and (ii)] that in turn correspond to the composite diffraction patterns shown in Fig. 1 and 2, respectively. In the former, three of the five subunits are aligned along crystallographic zones; the bottom subunit (T_1) along <100>, and T_3 and T_4 along <112> [Fig. 3b(i)]. In this model, the five end faces are all indexed as (111), such that T_1 diffracts along a [001] direction and T_3 and T_4 along [$\bar{1}$12] and [1$\bar{1}$2] directions, respectively. Corresponding reflections for the T_1 and T_3 domains are labelled in Fig. 1(b). The alternative orientation [Fig. 3b(ii)] also contains three diffracting subunits – T_5, along the <110> zone, and T_2 and T_3, along <111> – as depicted in Fig 2(b), in which the reflections for T_5 (along [1$\bar{1}$0]) and T_2 (along [1$\bar{1}\bar{1}$]) are specifically labelled. The two possible orientations for the penta-twinned rod are related by a rotation of 18° around the common <110> central axis, and the structural model was therefore confirmed by recording electron diffraction patterns on individual rods at different angles of tilt. The results showed that the two composite diffraction patterns could be obtained by tilting either of the zones through ±18°, as previously reported for copper nanorods.[27]

HRTEM studies gave lattice images that were consistent with the penta-twinned structure and orientation described above. Images recorded down the <112>/<100> zone showed well-defined continuous {111} fringes (d = 0.236 nm) running parallel to the direction of elongation on both sides of the rod, but which became modulated along the central region into larger electron dense stripes (Fig. 4). Fourier spectral analysis of line traces of the lattice fringes across the rod showed a {111} reflection across the entire width of the particle, and an additional d spacing of *ca.* 0.6 nm in the central regions. The latter was attributed to a double diffraction reflection arising from a combination of the (2$\bar{2}$2) and ($\bar{2}$20) spots in the [$\bar{1}$12] and [001] zones, respectively. The data indicated therefore that the superimposition of <112>/<100> zones occurred only in the central regions of the rods, which is consistent with the orientation shown in Fig. 3 b(i) where the T_3 and T_4 domains of the cyclic penta-twinned structure are aligned along the <112> zone across the width of the rod, and the overlap with the <100> zone of T_1 occurs only in the central region of the particle. In contrast, lattice images recorded down the <110>/<111> zone showed {111} fringes only on one side of the rod and at an angle of 55° to the [110] axis of elongation. These fringes originated solely from the T_5 subunit aligned along the [1$\bar{1}$0] zone.

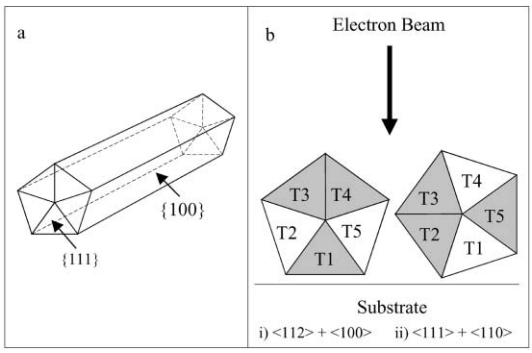

Fig. 3 Elongated cyclic penta-tetrahedral twin model of gold nanorods. (a) Idealized 3-D morphology showing {111} end faces and {100} side faces. The common five-fold axis of elongation is [110]. (b) Cross-section of nanorod structure showing arrangement of twins T1 to T5, and possible orientations of domains with respect to the electron beam. These give rise to superimposed zone combinations of (i) <112> and <100>, and (ii) <110> and <111> that are related in the diagram by an anticlockwise rotation of 18° around the five-fold <110> central axis. Twin domains in diffraction alignment are highlighted.

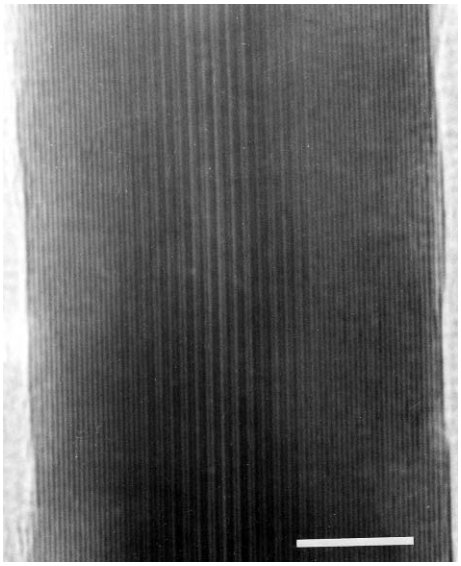

Fig. 4 HRTEM image of gold nanorod viewed down the <112>/<100> zone showing continuous {111} fringes (d = 0.236 nm) parallel to the direction of elongation. The fringes are modulated in the central region of the twinned crystal into wider stripes due to double diffraction arising from the superposition of twin domains aligned along different zones [see also Fig. 3b(i)]. Scale bar, 5 nm.

View Article Online

Published on 16 April 2002. Downloaded by Pennsylvania State University on 12/09/2016 10:55:22.

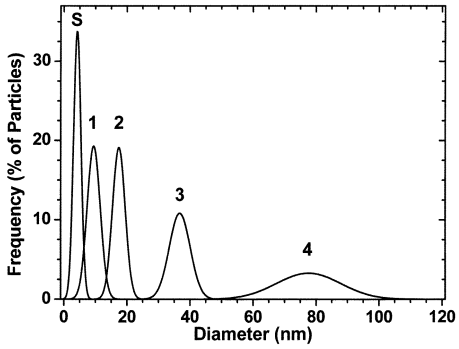

Fig. 5 Particle size Gaussian distributions for seed crystals (S) and isometric gold nanoparticles formed during the sequence of seed-mediated growth (tubes 1 to 4).

Growth

The growth stages associated with the formation of the twinned nanorods were elucidated by TEM studies on the structure, morphology and size distributions of particles isolated from the sequence of reaction mixtures used in the seed-mediated process (test-tubes 1–4, see experimental methods). Corresponding spectroscopic studies of the growth process have been recently published.[17] The seeds were prepared by $[BH_4]^-$ reduction of $[AuCl_4]^-$ and consisted of citrate-stabilized gold nanoparticles that were isotropic in shape and monodisperse in size (mean = 4.3 nm, σ = 1.2 nm). Interestingly, HRTEM lattice images indicated that the seed nanoparticles were not twinned but single domain crystals. Introduction of the seeds into the CTAB-containing reaction solution of tube 1 produced monodisperse isometric particles with increased dimension (mean = 9.6 nm, σ = 2.1 nm). The distinct shift rather than broadening of the particle size distribution (Fig. 5) indicated that growth of the seeds was favoured over primary nucleation of new particles, suggesting that disproportionation and reduction of the Au(I) and Au(III) complexes, respectively, are facilitated by binding to surface sites on the preformed crystallites. Significantly, TEM images showed that the growth of the seeds in tube 1 was associated with five-fold twinning in many of the gold nanoparticles [Fig. 6(a)]. Multiple twinning in gold often occurs for particles above 8 nm in size by coalescence of primary particles with tetrahedral morphology,[30] which is consistent with the above observations.

Transfer of particles formed in tube 1 into a fresh reaction solution (tube 2) resulted in a continued increase in the size of the isometric particles (mean = 17.4 nm, σ = 2 nm, Fig. 5), along with a low yield (4%) of monodisperse, rod-shaped nanoparticles [Fig. 6(b)]. The mean values for the width, length and aspect ratio were 15 nm (σ = 1.7 nm), 30 nm (σ = 4.0 nm), and 2.1 (σ = 0.4), respectively (Fig. 7a, 8a and 9a). Reiteration of this process but using particles from tube 2 increased the population of nanorods in tube 3 to 10%, with the remaining 90% comprising mainly monodisperse isometric twinned

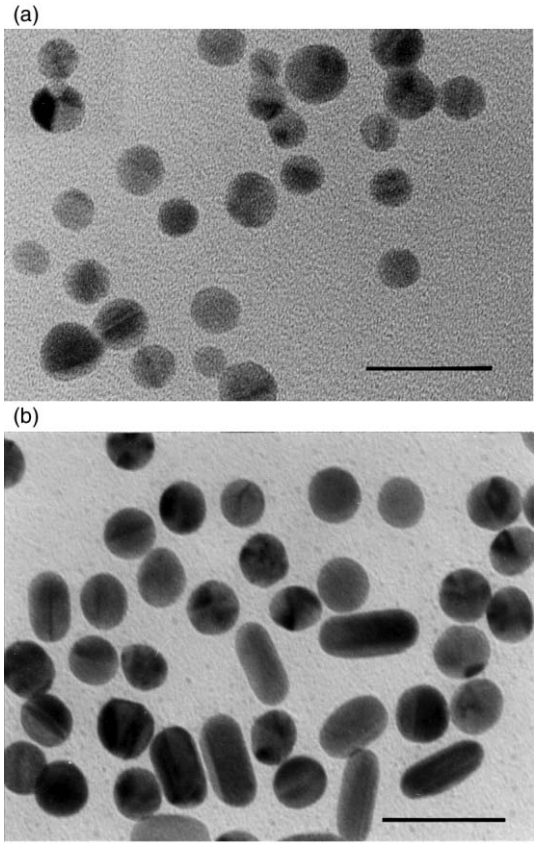

Fig. 6 TEM images of twinned gold nanoparticles: (a) tube 1, isometric crystals; (b) tube 2, short rods and isometric crystals. Scale bars, 20 and 50 nm, respectively.

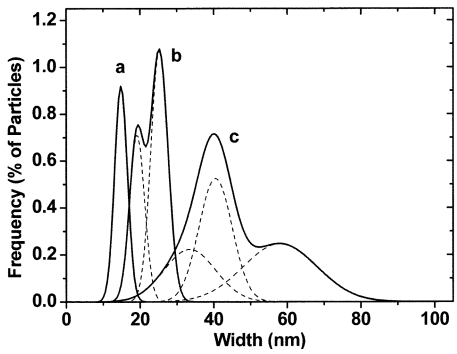

Fig. 7 Gaussian distributions of nanorod widths: (a) tube 2; (b) tube 3; (c) tube 4. Dashed curves show deconvoluted curves for nanorods in tubes 3 and 4.

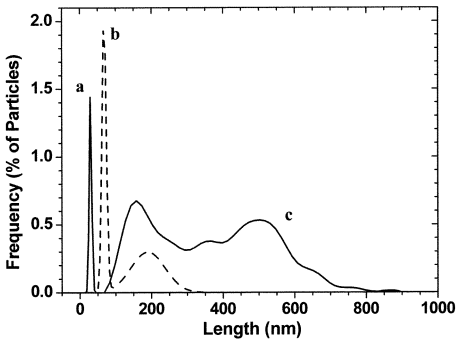

Fig. 8 Histograms of the nanorod lengths: (a) tube 2; (b) tube 3; (c) tube 4. Gaussian distributions are shown for tubes 2 and 3 only.

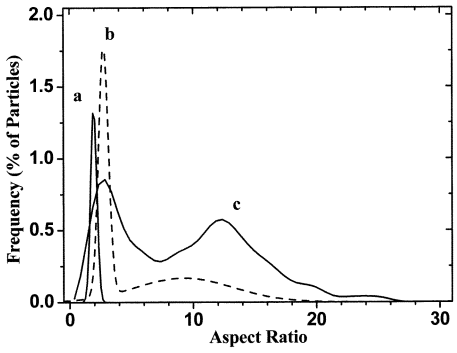

Fig. 9 Histograms of nanorod aspect ratios: (a) tube 2; (b) tube 3; (c) tube 4. Gaussian distributions are shown for tubes 2 and 3 only.

View Article Online

Published on 16 April 2002. Downloaded by Pennsylvania State University on 12/09/2016 10:55:22.

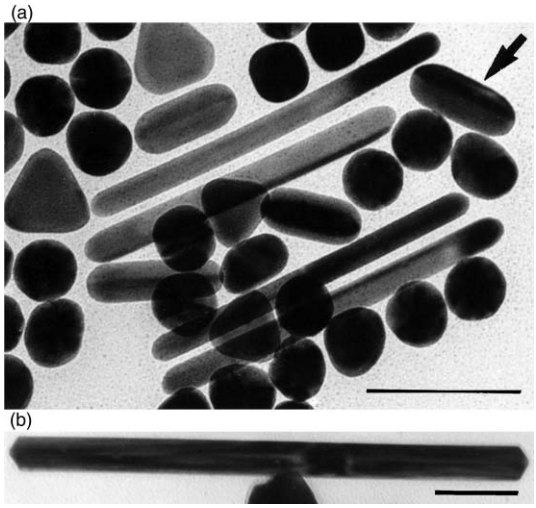

Fig. 10 TEM images of twinned gold nanoparticles: (a) tube 3, long and short (arrow) rods, isometric crystals and triangular plates; (b) tube 4, high aspect ratio nanorod with facetted end faces. Scale bars, 100 nm.

particles of increased size (mean = 36.7 nm, σ = 3.3 nm, Fig. 5) along with low numbers of triangular, plate-shaped crystals. As shown in Fig. 7b, the rod-shaped nanoparticles exhibited a bimodal distribution of widths. Approximately 40% of the nanorods were highly anisotropic [Fig. 10(a)], with a narrow width distribution (mean = 20 nm) and relatively high aspect ratio, although the latter ranged from values of 6 to 20 [Fig. 9(b)] due to a large spread in the particle lengths between 100 and 300 nm [Fig. 8(b)]. In comparison, the remaining 60% of the nanorods [see arrow in Fig. 10(a)] were larger in width (mean = 26 nm), significantly shorter in length (mean = 70 nm), and highly monodisperse (mean aspect ratio = 3.0, σ = 0.5).

A similar analysis of particles prepared in tube 4 showed a further increase in the percentage of rods to 16% and size of the isometric particles (mean = 77 nm, σ = 10.2 nm, Fig 5). The histogram of rod widths (Fig. 7c) was deconvoluted into three overlapping Gaussian distributions located at mean values of 34, 40 and 58 nm. The integrals of each distribution were 24, 37 and 39% of the rod population, respectively, which corresponded to approximately 4, 6 and 6% of the total particles produced in tube 4. Measurements of the corresponding particle lengths (Fig. 8c) showed that the nanorods increased in length within the range 150–800 nm, and that longer lengths were associated with shorter widths, such that highly anisotropic, needle-like twinned crystals with facetted end faces were observed [Fig. 10(b)]. The general increase in spread of the widths and lengths resulted in a high polydispersity in the aspect ratio, which ranged from 2 to 25 with maxima around values of 3 and 12 (Fig. 9c).

Discussion

Our results indicate that the shape anisotropy exhibited by gold nanorods synthesized by seed-mediated sequential growth in the presence of the cationic surfactant CTAB is determined by symmetry reduction associated with cyclic penta-twinning of the fcc lattice. The breaking of cubic symmetry arises by initial growth and aggregation of the seed crystals added to tube 1 to produce isometric twinned particles with a decahedral morphology based on ten well-defined {111} faces and five {100} side edges arranged around a common [110] central axis. This form of multiple twinning is relatively common for metals with fcc structures[29] although subsequent anisotropic growth of the isometric crystals to produce gold nanorods has not been documented. Previous studies have shown that copper and silver nanorods formed in microemulsions[27] and along stepped surfaces of NaCl,[23] respectively, are also twinned along five {111} planes, although few details of the growth mechanism were reported.

In our experiments, growth of the isometric twinned crystals in the presence of CTAB results in the initial transformation in tube 2 of *ca.* 4% of the twinned particles into short nanorods, while the remaining crystals increase in size to around 17 nm. Once formed, the nanorods grow almost unidirectionally in length when immersed in a fresh reaction solution (tube 3) to produce needle-shaped, penta-twinned particles with high aspect ratios and variable crystal lengths between 100 and 300 nm. Because the increase in width is marginal, the elongated crystals have a uniform thickness that is determined by the width of the short nanorods formed in the previous stage of the reaction sequence. Simultaneously, approximately 6% of the 17 nm-sized isometric twins are transformed into prolate particles that constitute a new population of short, rod-shaped nanoparticles, whilst the remaining crystals continue to grow isometrically.

Subsequent transfer of the products into fresh reaction solutions reiterates the combination of isometric growth, nanorod elongation and nanorod formation to produce a trimodal distribution in rod widths in reaction tube 4. The distribution corresponds to three types of nanorods with mean widths of 34 (type 1), 40 (type II) and 58 nm (type III) and decreasing aspect ratios with values in the ranges 17–20, 8–11, and 2–3, respectively. Each type can be correlated with the widths of the transferred needle-shaped, short rod-like or isometric nanoparticles, respectively, which in turn are related to the dimensions and shapes of crystals formed in earlier stages of the sequential process (Fig. 11).

In general, the formation of mixed populations of gold nanoparticles and their associated morphologies and sizes can be rationalized by differences in the delay in the onset of shape anisotropy in the reaction sequence. Clearly, the mechanism responsible for the transformation from isotropic to anisotropic growth of the isometric penta-twinned nanoparticles is not highly competitive, although once achieved, the crystals rapidly elongate along the common [110] axis, suggesting that the process is essentially auto-catalytic. As the unidirectional growth rate is high and the onset of the shape transformation process occurs over an extended reaction period, the nanorods originate at different times to produce a marked variation in the particle lengths. In contrast, the width of each particle increases only slowly, which indicates that the {100} side edges are effectively blocked from further growth compared with the {111} end faces. Previous studies have indicated that the yield of nanorods rises with an increased concentration of CTAB,[17] suggesting that CTAB molecules bind more strongly to the {100} edges than the {111} end faces, with the consequence

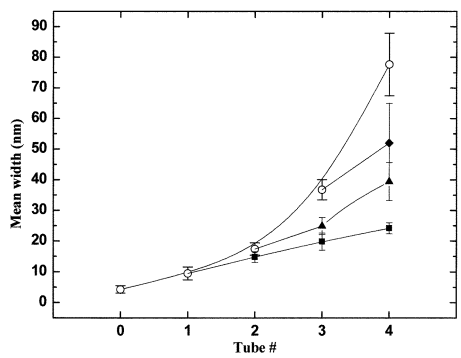

Fig. 11 Plot of the mean width of isometric particles and nanorods against tube number. The correlations between the onset of isometric transformation and subsequent nanorod growth are shown. This results in two and three distinct types of nanorods in tubes 3 and 4, respectively. (○) isometric, (■) type I nanorods, (▲) type II nanorods, and (◆) type III nanorods.

View Article Online

Published on 16 April 2002. Downloaded by Pennsylvania State University on 12/09/2016 10:55:22.

that the crystal grows preferentially along the [110] direction as the side edges/faces become stabilized. The HRTEM data suggest that this process is not specific enough to produce well-defined {100} side faces, particularly in the initial stages of nanorod formation.

It seems likely that structural and chemical factors play an important role in determining the preferential interactions between the cationic quaternary ammonium headgroups and growth sites on the side edges and faces. Previously, complexes of $[AuCl_4]^-$ and cationic surfactants have been shown to produce gold colloids in which the particle size decreases on increasing the surfactant concentration due to enhanced surface adsorption and growth inhibition.[31] It seems likely therefore that similar surfactant-containing complexes as well as those involving Au(I) species, such as $[AuBrCTA]^+$, are specifically incorporated into the {100} side edges, whereas non-complexed ion-pairs or Au(0) atoms/clusters are added to the {111} end faces. The discrimination between sites could be due to the increased stability of the close-packed {111} surfaces compared with the edge sites, which will contain numerous defects. Moreover, binding of the large $[NMe_3]^+$ headgroup (diameter = 0.814 nm, area = 0.521 nm^2)[32] and associated long alkyl chain can be more readily accommodated around the edges of the isometric penta-twinned crystals than within the plane of individual {111} faces, where the Au–Au spacings are too small to facilitate epitaxy. As the nanorods grow in length, the area of the side faces increases, and this could facilitate the assembly of a bilayer of surfactant molecules at the crystal surface.[33] In turn, the bilayer would provide additional stabilization and growth inhibition, and this could explain why elongation of the nanorods is rapid once the shape anisotropy has been established.

Finally, we note that our proposed mechanism follows a classical description of crystal growth inhibition that involves the attachment of individual surfactant molecules to the side edges/faces of cyclic, penta-twinned gold nanoparticles. The mechanism does not implicate the involvement of surfactant micelles in controlling the shape anisotropy of fcc metallic nanoparticles, as has been previously postulated.[17,22,24] Instead, the data presented here clearly indicate that symmetry breaking in fcc metallic structures is an intrinsic structural mechanism (twinning) that is subsequently modulated extrinsically during growth in solution by edge-specific surfactant adsorption. This mechanism appears to be sufficiently general that it could also apply to other experimental procedures, such as electrochemical reduction[19] or the use of microemulsions,[24] both of which contain charged surfactants and produce high aspect ratio metallic nanoparticles.

Acknowledgements

We thank the EPSRC, UK for support of a postgraduate studentship to C. J., the European Union for a Marie Curie Individual Fellowship (HPMF-CT-1999-00254) to E. D, and the US National Science Foundation for funding to C. J. M.

References

1 J. H. Fendler, *Nanoparticles and Nanostructured Films*, Wiley-VCH, Weinheim, 1998.
2 N. Shipway, E. Katz and I. Willner, *ChemPhysChem*, 2000, **1**, 18.
3 J. Fink, C. J. Kiely, D. Bethell and D. J. Schiffrin, *Chem. Mater.*, 1998, **10**, 922.
4 Z. L. Wang, *Adv. Mater.*, 1998, **10**, 13.
5 R. L. Whetten, M. N. Shafigullin, J. T. Khoury, T. G. Schaaff, I. Vezmar, M. M. Alvarez and A. Wilkinson, *Acc. Chem. Res.*, 1999, **32**, 397.
6 P. C. Ohara and W. M. Gelbart, *Langmuir*, 1998, **14**, 3418.
7 P. C. Ohara, J. R. Heath and W. M. Gelbart, *Angew. Chem., Int. Ed. Engl.*, 1997, **36**, 1078.
8 S.-W. Chung, G. Markovich and J. R. Heath, *J. Phys. Chem. B*, 1998, **102**, 6685.
9 P. C. Hidber, W. Helbig, E. Kim and G. M. Whitesides, *Langmuir*, 1996, **12**, 1375.
10 S. L. Burkett and S. Mann, *Chem. Commun.*, 1996, 321.
11 R. W. Zehner, W. A. Lopes, T. L. Monkved, H. Jaeger and L. R. Sita, *Langmuir*, 1998, **14**, 241.
12 M. Li, H. Schnablegger and S. Mann, *Nature*, 1999, **402**, 393.
13 B. Nikoobakht, Z. L. Wang and M. A. El-Sayed, *J. Phys. Chem. B*, 2000, **104**, 8635.
14 B. A. Korgel and D. Fitzmaurice, *Adv. Mater.*, 1998, **10**, 661.
15 X. Peng, L. Manna, W. Yang, J. Wickham, E. Scher, A. Kadavanich and A. P. Alivisatos, *Nature*, 2000, **404**, 59.
16 L. Manna, E. C. Scher and A. P. Alivisatos, *J. Am. Chem. Soc.*, 2000, **122**, 12 700.
17 N. R. Jana, L. Gearheart and C. J. Murphy, *J. Phys. Chem. B*, 2001, **105**, 4065.
18 N. R. Jana, L. Gearheart and C. J. Murphy, *Adv. Mater.*, 2001, **13**, 1389.
19 Y. Y. Yu, S. S. Chang, C. L. Lee and C. R. C. Wang, *J. Phys. Chem. B*, 1997, **101**, 6661.
20 S. S. Chang, C. W. Shih, C. D. Chen, W. C. Lai and C. R. C. Wang, *Langmuir*, 1999, **15**, 701.
21 M. J. Yacaman, J. A. Ascencio and G. Canizal, *Surf. Sci.*, 2001, **486**, L449.
22 N. R. Jana, L. Gearheart and C. J. Murphy, *Chem. Commun.*, 2001, 617.
23 S. A. Nepijko, D. N. Levlev, W. Schulze, J. Urban and G. Ertl, *ChemPhysChem*, 2000, **1**, 140.
24 M. P. Pileni, T. Gulik-Krzywicki, J. Tanori, A. Filankembo and J. C. Dedieu, *Langmuir*, 1998, **14**, 7359.
25 N. Cordente, M. Respaud, F. Senocq, M.-J Casanove, C. Amiens and B. Chaudret, *Nano Lett.*, 2001, **1**, 565.
26 Z. L. Wang, M. B. Mohamed, S. Link and M. A. El-Sayed, *Surf. Sci.*, 1999, **440**, L809–814.
27 I. Losiecki, A. Filankembo, H. Sack-Kongehl, K. Weiss, M. P. Pileni and J. Urban, *Phys. Rev. B*, 2000, **61**, 4968.
28 S. Weaver, D. Taylor, W. Gate and G. Mills, *Langmuir*, 1996, **12**, 4618.
29 L. D. Marks, *Rep. Prog. Phys*, 1994, **57**, 603.
30 K. Yagi, K. Takayanagi, K. Kobayashi and G. Honjo, *J. Cryst. Growth*, 1975, **28**, 117.
31 H. Ishizuka, T. Tano, K. Torigoe, K. Esumi and K. Meguro, *Colloids Surf.*, 1992, **63**, 337.
32 L. T. Okano, F. H. Quina and O. A. El Seoud, *Langmuir*, 2000, **16**, 3119.
33 B. Nikoobakht and M. A. El-Sayed, *Langmuir*, 2001, **17**, 6368.